PHYSICAL REVIEW D **85,** 035006 (2012)

Assessing the discovery potential of directional detection of dark matter

J. Billard,* F. Mayet, and D. Santos

Laboratoire de Physique Subatomique et de Cosmologie, Université Joseph Fourier Grenoble 1, CNRS/IN2P3, Institut Polytechnique de Grenoble, Grenoble, France

(Received 27 October 2011; published 7 February 2012)

There is a worldwide effort toward the development of a large time projection chamber devoted to directional dark matter detection. All current projects are being designed to fulfill a unique goal: identifying weakly interacting massive particle (WIMP) as such by taking advantage of the expected direction dependence of WIMP-induced events toward the constellation Cygnus. However, such proof of discovery requires a careful statistical data treatment. In this paper, the discovery potential of forthcoming directional detectors is addressed by using a frequentist approach based on the profile likelihood ratio test statistic. This allows us to estimate the expected significance of a dark matter detection taking into account astrophysical and experimental uncertainties. We show that the energy threshold and the background contamination are key experimental issues for directional detection, while angular resolution and sense recognition efficiency only mildly affect the sensitivity and the energy resolution is unimportant. This way, we found that a 30 kg.year CF_4 directional experiment could reach a 3σ sensitivity at 90% C.L. down to 10^{-5} pb and 3.10^{-4} pb for the WIMP-proton axial cross section in the most optimistic and pessimistic detector performance case, respectively.

DOI: 10.1103/PhysRevD.85.035006 PACS numbers: 95.35.+d, 14.80.−j

I. INTRODUCTION

An ever increasing body of evidence supports the existence of cold dark matter as the major contribution to the matter budget of the Universe. On the largest scale, cosmological measurements [1] tightly constrain the cold dark matter relic density whereas on a local scale, the discrepancy between the rotation curves of spiral galaxies, as measured by 21 cm observations, and the ones that would be inferred from the luminous matter, indicates that spiral galaxies, including the Milky Way, should be embedded in a dark matter halo [2,3].

Directional detection of galactic dark matter has been proposed as a powerful tool to identify genuine weakly interacting massive particle (WIMP) events as such [4]. Indeed, one expects a clear asymmetry in the angular distribution of WIMP-induced events in the direction of motion of the Solar System, which happens to be roughly in the direction of the constellation Cygnus. As the background distribution is expected to be isotropic in the galactic rest frame, one expects a clear and unambiguous difference between the WIMP-induced signal and the background one. Recent studies have shown that, within the framework of dedicated statistical data analysis, a low-exposure directional detector could lead either to a high-significance discovery of galactic dark matter [5–7] or to a competitive exclusion [8]. Nondirectional direct detection of dark matter is entering in a new era as several detectors are starting to exclude the upper part of the predicted supersymmetric parameter space, either in the spin-independent channel [9–12] or in the spin-dependent one [13–20]. On the other hand, forthcoming directional detection projects are designed to claim a proof of discovery. Both approaches require a dedicated statistical treatment, taking into account systematics related to detector performance as well as astrophysical uncertainties. Following [21,22], we use a profile likelihood ratio test statistic to assess the discovery potential of directional detection.

We give a complete overview of the effect of the main experimental issues on the discovery potential of directional detection of dark matter. Our aim is to establish a weighted wish list that could be used when trying to optimize the design of a dark matter directional detection experiment. The experimental issues considered hereafter are the background contamination, the energy threshold, the sense recognition efficiency, the angular resolution, the energy resolution, and the background modeling. With a profile likelihood method, we estimate the sensitivity of a given directional experiment by taking into account the most relevant astrophysical uncertainties, e.g. the local dark matter density, the WIMP velocity distribution, and the velocity of the Solar System orbit.

The paper is organized as follows. Section II presents a brief introduction of directional dark matter detection, both from an experimental point of view and from a theoretical one. Section III introduces the definition of the likelihood function we have used, as well as the formalism of a frequentist approach to estimate the significance with a profile likelihood ratio test statistic. Section IV focuses on the application of the profile likelihood test to estimate the impact of the different experimental issues on the sensitivity of upcoming directional detector. Finally, in Sec. V we conclude this study by considering two very

*billard@lpsc.in2p3.fr

different detectors with their respective performance to evaluate both their sensitivity to dark matter from supersymmetric models and their competitivity in comparison to existing limits.

II. DIRECTIONAL DETECTION FRAMEWORK

A. Detector configuration

There is a worldwide effort toward the development of a large time projection chamber (TPC) devoted to directional detection [23] and all current projects [24–29] face common experimental challenges and share a unique goal: the simultaneous measurement of the energy (E_r) and the three-dimensional (3D) track (Ω_r) of low-energy recoils, thus allowing to evaluate the double-differential spectrum $\mathrm{d}^2R/\mathrm{d}E_r\mathrm{d}\Omega_r$ down to the energy threshold. This can be achieved with low-pressure gaseous detectors (TPC) and several gases have been suggested: CF_4, ^3He, C_4H_{10}, or CS_2. As a matter of fact, experimental key issues include: sense recognition [30–32], angular and energy resolutions, energy threshold, as well as the residual background contamination. Bearing in mind the need for a directional detector optimization [8,33] at the current stage of detector design, we present in Sec. IV a study of the effect of detector configurations in the case of a working example: a low-exposure (30 kg.year) CF_4 TPC, operated at low pressure and allowing 3D track reconstruction as proposed by the MIMAC collaboration [29].

B. Directional detection

Directional detection depends crucially on the local WIMP velocity distribution [34–36]. The isothermal sphere halo model is often considered but it is worth going beyond this standard paradigm when trying to account for all astrophysical uncertainties. The multivariate Gaussian WIMP velocity distribution corresponds to the generalization of the standard isothermal sphere [37] with a density profile $\rho(r) \propto 1/r^2$, leading to a smooth WIMP velocity distribution, a flat rotation curve, and no substructure. The WIMP velocity distribution in the laboratory frame is given by

$$f(\vec{v}) = \frac{1}{(8\pi^3 \det\boldsymbol{\sigma}_v^2)^{1/2}} \exp\left[-\frac{1}{2}(\vec{v}-\vec{v}_\odot)^T \boldsymbol{\sigma}_v^{-2}(\vec{v}-\vec{v}_\odot)\right], \tag{1}$$

where $\boldsymbol{\sigma}_v = \mathrm{diag}[\sigma_x, \sigma_y, \sigma_z]$ is the velocity dispersion tensor assumed to be diagonal in the Galactic rest frame $(\hat{x}, \hat{y}, \hat{z})$ and $\vec{v}_\odot$ is the Sun's velocity vector with respect to the Galactic rest frame. When neglecting the Sun peculiar velocity and the Earth orbital velocity about the Sun, $\vec{v}_\odot$ corresponds to the detector velocity in the Galactic rest frame and is taken to be $v_\odot = 220$ km.s^{-1} along the $\hat{y}$ axis pointing toward the Cygnus constellation at ($\ell_\odot = 90°$, $b_\odot = 0°$). The directional recoil rate is given by [38]

$$\frac{\mathrm{d}^2R}{\mathrm{d}E_r\mathrm{d}\Omega_r} = \frac{\rho_0\sigma_0}{4\pi m_\chi m_r^2} F^2(E_r)\hat{f}(v_{\min}, \hat{q}), \tag{2}$$

with m_χ the WIMP mass, m_r the WIMP-nucleus reduced mass, ρ_0 the local dark matter density, σ_0 the WIMP-nucleus elastic scattering cross section, $F(E_r)$ the form factor (using the axial expression from [39]), $v_{\min}$ the minimal WIMP velocity required to produce a nuclear recoil of energy E_r, and $\hat{q}$ the direction of the recoil momentum. Finally, $\hat{f}(v_{\min}, \hat{q})$ is the three-dimensional Radon transform of the WIMP velocity distribution $f(\vec{v})$. Using the Fourier slice theorem [38], the Radon transform of the multivariate Gaussian is

$$\hat{f}(v_{\min}, \hat{q}) = \frac{1}{(2\pi\hat{q}^T\boldsymbol{\sigma}_v^2\hat{q})^{1/2}} \exp\left[-\frac{[v_{\min} - \hat{q}.\vec{v}_\odot]^2}{2\hat{q}^T\boldsymbol{\sigma}_v^2\hat{q}}\right]. \tag{3}$$

As outlined in [5–7], a clear and unambiguous signature in favor of a dark matter detection is given by the fact that the recovered main recoil direction is shown to be pointing toward Cygnus within a few degrees. However, to assess the significance of the discovery, in a frequentist approach and taking into account astrophysical uncertainties, a complete statistical analysis is required, as outlined below.

C. Astrophysical uncertainties

The effect of astrophysical parameters on exclusion limits deduced from direct detection, both from energy, annual modulation, and direction measurements, has been investigated in detail in [8,35,36,40–45]. For a complete discussion on their evaluations, uncertainties, and effect on dark matter detection, we refer the reader to [46,47] and references therein. For dark matter search, both direct and directional, it is indeed of great interest to account for uncertainties on astrophysical parameters, as in [22], although it has been done for the escape velocity only, within the framework of a profile likelihood ratio test statistic. Three astrophysical parameters play a key role: the local dark matter density ρ_0, the Sun's velocity vector $v_\odot$, and the WIMP velocity distribution, parametrized by the velocity dispersions along the three axes $\sigma_{x,y,z}$.

As the WIMP event rate is proportional to the quantity $\rho_0 \times \sigma_p$, the value of the local dark matter density ρ_0 directly affects the estimation of the WIMP-proton cross section σ_p. A standard value $\rho_0 = 0.3$ GeV.c^{-2} is usually used for the sake of comparison of various direct detector results [48,49]. However, there are still debates on the value of ρ_0 and several papers, using different techniques, have found the following values of the local dark matter density: $\rho_0(\mathrm{GeV/c^2/cm^3})$ equal to 0.32 ± 0.07 [45], $0.43 \pm 0.11 \pm 0.10$ [50], 0.3 ± 0.1 [51], and 0.39 ± 0.03 [52]. Clearly, systematic errors arise from uncertainties in modeling the Milky Way. Interestingly, S. Garbari *et al.* [53] point out that it is vital to measure the vertical dispersion profile of the tracers to recover an unbiased estimate of ρ_0. Depending on the choice of the velocity distribution of

star tracer population (from isothermal to nonisothermal), their estimation of ρ_0 can vary by a factor of 10 or so. Recently, M. C. Smith *et al.* [54] have computed a local dark matter density of 0.57 GeV/c^2/cm^3 using Sloan Digital Sky Survey data [55] by studying the kinematics of Galactic disk stars in the solar neighborhood.

Valuable information are also extracted from recent high-resolution N-body simulations of Milky-Way-like objects. In particular, it is shown in [56] that the estimation of the local dark matter density, on the stellar disk and at $\sim$8 kpc from the Galactic center, is found to be always larger, by 20% or so, than the average density in a spherical shell of same radius, i.e the above quoted quantity inferred from dynamical measurements. Interestingly, the local dark matter density distribution is predicted [57] to be remarkably smooth, varying by less than 15% at the 99.9% C.L. from the average value over an ellipsoidal shell. This highlights the fact that the local density, at the Sun's location, should not differ from the above estimations.

These arguments, both from observations and simulations, add still more weights to the need of taking a possible range of values for the local dark matter density rather than a fixed standard value ($\rho_0 = 0.3$ GeV.c^{-2}), although it allows a fair comparison of various dark matter search results. Hence, to account for all estimations and uncertainties, the local dark matter density ρ_0 is treated hereafter as a nuisance parameter in the following, considering the range 0.3 ± 0.1 GeV/c^2/cm^3, see Table I.

On the choice of mean value and uncertainty, it is worth emphasizing that the local dark matter density is indeed a key experimental issue for directional dark matter search (as for direction-insensitive one) but its effect is rather simple to handle. For instance, taking a larger value (e.g. as proposed by [54]), say 0.4 instead of 0.3, will mainly change the sensitivity by 33%, giving in fact a sensitivity to smaller cross sections. For a study aiming at showing the reach of directional detection, a modification of the range chosen for the local dark matter density does not affect the result. This is not the case however, when presenting an experimental result as outlined above.

The second astrophysical parameter to be carefully handled is the Sun's velocity $v_\odot$ equal to the local circular speed when neglecting the Sun's peculiar velocity. The standard value is 220 ± 20 km.s^{-1} [58]. As outlined in [41,46,47], recent determinations of its value span on a wide range and the impact on directionality has been studied [8,59]. Several papers, using different techniques, have studied the value of local circular speed, giving slightly different values. They found $v_\odot$ (km.s^{-1}) equal to 254 ± 16 [60], 200–280 [61], 236 ± 11 [62], 221 ± 18 [63], and 218 ± 7 [64]. It is worth noticing that the evaluation of the Sun's circular velocity depends crucially on the value of the distance of the Sun to the galactic center (R_0), which is also poorly known: $R_0 = 8.4 \pm 0.4$ kpc [65] and $R_0 = 8.33 \pm 0.35$ kpc [66]. In the following, the local circular speed is treated as a nuisance parameter, considering the range 220 ± 30 km.s^{-1}, see Table I.

TABLE I. Gaussian parametrization (mean and standard deviation) of the different astrophysical nuisance parameters.

Nuisance parameters	Gaussian parametrization
ρ_0 [GeV/c^2/cm^3]	0.3 ± 0.1
$v_\odot$ [km/s]	220 ± 30
σ_x [km/s]	$220/\sqrt{2} \pm 20$
σ_y [km/s]	$220/\sqrt{2} \pm 20$
σ_z [km/s]	$220/\sqrt{2} \pm 20$

Finally, uncertainties in the local WIMP velocity distribution must be accounted for. The effect of halo modeling on exclusion limits and allowed regions has been studied [7,67]. Indeed, recent results from N-body simulations are in favor of triaxial dark matter haloes with anisotropic velocity distributions and potentially containing substructure as subhaloes (clumps) and dark disk [40,68–71]. Moreover, recent observations of Sagittarius stellar tidal stream have shown evidence for a triaxial Milky Way dark matter halo [72]. However, it is noteworthy that this result holds true at large radius (60 kpc) and N-body simulations have shown that there can be significant variations of the axis ratios with radius [73]. S. H. Hansen and B. Moore identified a universal relation between the radial density slope and the velocity anistropy leading to $\beta \sim 0.1$ at the solar neighborhood [74]. Using a sample of 1700 solar neighborhood halo subdwarfs from the Sloan Digital Sky Survey [55], M. C. Smith *et al.* have evaluated the halo velocity dispersion and found the anisotropy parameter β to be $\sim$0.5 [75]. Interestingly, the stellar halo exhibits no net rotation.

Even if it should be noticed that halo stars have *a priori* a different density profile from the dark matter, these facts can be taken as hints in favor of an anisotropic dark matter velocity distribution. To account for this effect, we consider a multivariate Gaussian WIMP velocity distribution, i.e. anisotropic, but without substructures. It is parametrized by the velocity dispersions $\sigma_{x,y,z}$. Effect of non-smooth halo model with substructures and/or streams will be addressed in a forthcoming paper. The velocity anisotropy $\beta(r)$ is defined as [76]

$$\beta(r) = 1 - \frac{\sigma_y^2 + \sigma_z^2}{2\sigma_x^2}. \tag{4}$$

According to N-body simulations with or without baryons [40,42,77–79], the β parameter at a radius $R_\odot \simeq 8$ kpc from the Galactic center spans the range 0–0.4, which is in favor of radial anisotropy. Indeed, such radial anisotropy is expected as the gravitational potential is mainly a function of the radius. In the following, the velocity dispersions $\sigma_{x,y,z}$ are treated as nuisance parameters, considering the range $220/\sqrt{2} \pm 20$ km/s, see Table I, which corresponds to $\beta = 0 \pm 0.25$. We used a null mean value of the velocity

anisotropy for the sake of comparison with other experiments, but the large uncertainty considered enables us to account for anisotropic halo model when computing the discovery potential of directional experiments. Moreover, as shown in [7], the effect of an extremely anisotropic halo model with $\beta = 0.4$ can be handled with such parametrization of the WIMP velocity distribution, as long as it can be approximated by a multivariate Gaussian, without introducing bias in the estimation of the WIMP properties (mass and cross section).

In this study, we have not used the escape velocity $v_{\rm esc}$ as an astrophysical nuisance parameter, since directional detection with low-energy threshold is almost insensitive to this parameter. Indeed, in the case of a WIMP mass of 100 GeV/c^2 the minimal speed to produce a 5 keV fluorine recoil is 130 km.s^{-1}, far below the median value of [80] equal to 544 km/s. Thus, the impact of $v_{\rm esc}$ is relevant for heavy targets and low WIMP mass in the so-called threshold region, where the experiment is only sensitive to the tail of the WIMP velocity distribution. In the following, we have considered an escape velocity taken as infinity to simplify the calculations.

As a conclusion, the use of a profile likelihood ratio test statistic allows us to account for uncertainties on the astrophysical parameters, as they are treated as nuisance parameters. This approach is a step beyond the ''standard dark matter halo paradigm,'' i.e. isotropic isothermal dark matter halo with fixed value of density. Evaluating the properties of the dark matter halo is indeed still a subject of debates and directional detection could bring valuable information, such as an evaluation of the anisotropy parameter, as shown in [7].

III. THE PROFILE LIKELIHOOD RATIO TEST STATISTIC

We are interested in estimating the expected significance of a discovery of dark matter with directional detection. In this section, we first introduce the definition of the likelihood function that we have used. In particular, astrophysical uncertainties are accounted for. Then, the formalism of a frequentist approach to estimate the significance using a profile likelihood ratio test statistic is presented. Finally, the impact of astrophysical uncertainties in the estimation of the significance is presented in a benchmark case.

A. The likelihood function

When considering directional detection of dark matter, the event distribution is given by the double-differential spectrum [Eq. (2)], which is a function of both the recoil energy and direction. On the other hand, the background event distribution is expected to be isotropic and will be considered as flat in energy unless otherwise stated. In this study, we are also taking into account five different astrophysical uncertainties as the local dark matter density ρ_0, the circular velocity of the Sun $v_\odot$, and the velocity dispersion along the three axes of the halo $\{\sigma_x, \sigma_y, \sigma_z\}$. Then, considering the extended definition of the likelihood function (see Ref. [81]) to take into account the Poisson statistics of the number of observed events N and the likelihood terms associated with each nuisance parameters, the full likelihood function is defined as

$$\mathcal{L}(\sigma_p, R_b, \vec{\nu}) = \frac{(\mu_s + \mu_b)^N}{N!} e^{-(\mu_s+\mu_b)} \prod_{n=1}^{N} \left[\frac{\mu_s}{\mu_s + \mu_b} S(\vec{R}_n) + \frac{\mu_b}{\mu_s + \mu_b} B(\vec{R}_n) \right] \prod_{i=1}^{5} \mathcal{L}_i(\nu_i), \quad (5)$$

where $\vec{\nu} = \{\rho_0, v_\odot, \sigma_x, \sigma_y, \sigma_z\}$ represents the set of nuisance parameters, $\mu_b = R_b \times \xi$ and μ_s correspond to the number of expected background and WIMP events, respectively, where ξ corresponds to the exposure. N is the total number of observed events, $\vec{R}_n$ refers to the energy and direction of each event while the functions S [see Eq. (2)] and B [isotropic distribution for the angular part and following Eq. (15) for the energy part] are the directional event rate $d^2R/dE_R d\Omega_R$ of the WIMP and background events, respectively. The functions $\mathcal{L}_i(\nu_i)$ refer to the likelihood function associated with each astrophysical nuisance parameter. They are considered as Gaussian functions with the parametrization from Table I.

B. The profile likelihood ratio

The significance of a new process, in a frequentist approach, is commonly estimated by using the profile likelihood ratio test. We present hereafter a brief overview of the subject by recalling basic relations for the reader's convenience. We refer to [21] for a comprehensive discussion. The profile likelihood ratio test corresponds to a hypothesis test against the null hypothesis H_0 (background only) against the alternative H_1, which includes both background and signal. The strength of the profile likelihood ratio relies in the fact that one can add some nuisance parameters both from an experimental side (efficiencies, resolutions, ...) and from a theoretical side (signal or background modeling). In our case, the H_0 hypothesis corresponds to the $\sigma_p = 0$ case (background only), while the alternative H_1 corresponds to the case where σ_p is taken different from 0 (background and signal). Then, in the case of a discovery, we test the background only hypothesis on the observed data and try to reject it using the following ratio:

$$\lambda(0) = \frac{\mathcal{L}(\sigma_p = 0, \hat{\hat{R}}_b, \hat{\hat{\vec{\nu}}})}{\mathcal{L}(\hat{\sigma}_p, \hat{R}_b, \hat{\vec{\nu}})}. \quad (6)$$

As discussed in [21], the test statistic in such case is defined as

$$q_0 = \begin{cases} -2\ln\lambda(0) & \hat{\sigma}_p > 0 \\ 0 & \hat{\sigma}_p < 0 \end{cases}. \quad (7)$$

As it can be seen from the previous equations, $0 \leq \lambda(0) \leq 1$ and $q_0 \geq 0$. Large value of q_0 implies a large discrepancy between the two hypotheses, which is in favor of a discovery. The p value p_0 is defined as

$$p_0 = \int_{q^{\rm obs}}^{\infty} f(q_0|H_0)dq_0, \quad (8)$$

where $f(q_0|H_0)$ is the probability density function of q_0 under the background-only hypothesis H_0. Then, p_0 corresponds to the probability to have a discrepancy, between H_0 and H_1, larger or equal to the observed one $q^{\rm obs}$. As an example, a p value of $p_0 = 0.001\,35$ corresponds to a 3σ signal observation. The main issue here is to have a correct estimation of the $f(q_0|H_0)$ distribution in order to compute the significance for a given data set. However, following Wilk's theorem, q_0 asymptotically follows a χ^2 distribution with one degree of freedom, see [21]. Then, in such case, the discovery significance Z is simply defined as $Z = \sqrt{q^{\rm obs}}$, in units of σ, i.e. $Z = 1$ corresponds to a significance of 68%. Figure 1 presents the probability density functions $f(q_0|H_0)$ of q_0 under the background-only hypothesis H_0 with/without astrophysical uncertainties. It is worth noticing that $f(q_0|H_0)$ is very well fitted by the χ^2_1 distribution. Indeed, in both cases: with and without astrophysical uncertainties, corresponding to the blue and black histograms, we found χ^2/d.o.f equal to 95.27/99 and 99.79/99, respectively.

C. Impact of astrophysical uncertainties

We aim at evaluating the discovery potential of upcoming directional detection experiment as a function of their experimental performance (resolutions, threshold, sense recognition) taking into account astrophysical uncertainties (see Sec. II C). In the following, we estimate the impact of the latter by studying two different cases: with and without uncertainties from astrophysics. Not considering the latter corresponds to remove the $\mathcal{L}_i$ functions from Eq. (5) and to consider all the astrophysical parameters as perfectly known (without error bars). To do the comparison, we ran 10 000 Monte Carlo simulations of a benchmark model with 100 WIMP events and 50 background events with a WIMP mass of 50 GeV/c^2. The distributions of the significance Z corresponding to the two scenarios are presented in Fig. 2. The black dashed histogram corresponds to the case without uncertainties and the blue solid one corresponds to the case where the uncertainties are taken into account. One can easily deduce that the mean value of the significance E(Z) is almost the same, i.e. 9.3 and 9.2, respectively. However, as shown in Fig. 2, the spread of the Z distribution is much wider when taking astrophysical uncertainties into account. This leads to a large difference between the two cases when considering a confidence level on the value of Z. Indeed, we defined Z_{90} as the value of the significance that could be at least reached by an experiment 90% of the time. Then, Z_{90} is found by solving the following equation:

$$\int_0^{Z_{90}} f(Z)dZ = 0.9, \quad (9)$$

where $f(Z)$ corresponds to the normalized distribution of the significance Z. Then, the value of Z_{90} with/without taking into account the astrophysical uncertainties is 5.9 and 7.9, respectively, leading to a large effect on the expected sensitivity to dark matter of a directional detector.

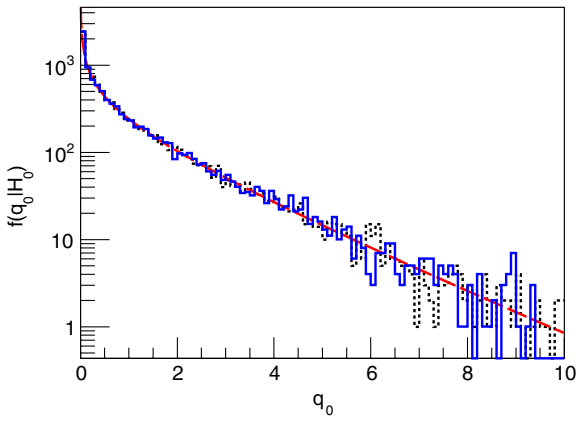

FIG. 1 (color online). Probability density functions of q_0 under the background-only hypothesis H_0 with/without (blue solid line/black dotted line) considering astrophysical uncertainties, estimated with 10 000 Monte Carlo simulations. The red long-dashed line corresponds to the χ^2_1 distribution.

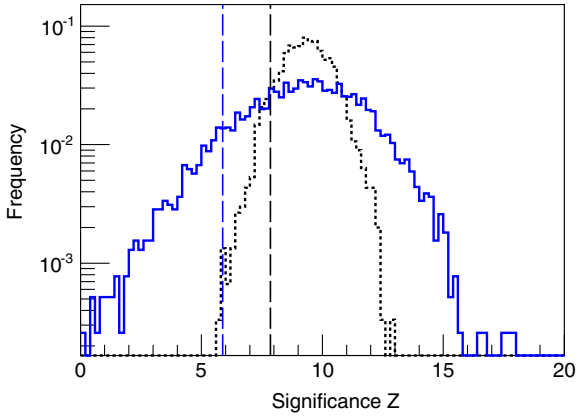

FIG. 2 (color online). Normalized distributions of the significance $f(Z)$ with/without (blue solid line/black dotted line) considering astrophysical uncertainties. Distributions were generated using 10 000 Monte Carlo simulations with 100 WIMP events and 50 background events with a WIMP mass $m_\chi = 50$ GeV/c^2. We found mean values of the significance of 9.2 and 9.3 and a 90% confidence lower limit Z_{90} of 7.9 and 5.9, respectively.

As a conclusion, this highlights the fact that it is necessary to take into account astrophysical uncertainties when estimating the sensitivity of a given directional detection experiment to dark matter. In the following, we define the sensitivity of a given directional experiment by the lower bound of the 3σ discovery region at 90% confidence level, given by the $Z_{90} = 3$ limit in the $(m_\chi, \log_{10}(\sigma_p))$ plane.

IV. OPTIMIZING DIRECTIONAL DETECTION

All current directional projects [24–29] face common challenges. As a matter of fact, experimental key issues include sense recognition [30–32], angular and energy resolutions, energy threshold, as well as the residual background contamination.

In this section, we evaluate the evolution of the significance of a discovery as a function of the detector performance. In a first place, we will be interested in the effect of the number of WIMP and background events in the data. Then, in a second part, we will consider some experimental issues, like the energy threshold $E_{\rm th}$, the angular resolution σ_γ, the sense recognition efficiency, the energy resolution σ_{E_r}, and the energy background modeling. In the following, we consider the mean significance E(Z) and the sensitivity, estimated from the limit corresponding to $Z_{90} = 3$ in the $(m_\chi, \log_{10}(\sigma_p))$ plane, using 1000 Monte Carlo simulations for each given set of input parameters. Unless otherwise stated, we consider a 10 kg CF_4 directional detector with a recoil energy range of [5, 50] keV with perfect angular and energy resolutions and with sense recognition. To study one by one the impact of a given experimental issue on the sensitivity, this parameter will be degraded keeping all other ones unchanged.

A. Residual background contamination

Zero background is often referred to as the ultimate goal for the next generation of direct detection experiments in deep underground laboratories. However, owing to the large intrinsic difference between the WIMP-induced and background-induced spectra, directional detection could accommodate to a sizeable background contamination. In this section, we investigate the effect of a residual background contamination, i.e. in the final data set after all selections based e.g. on track-length versus energy and fiducialization. Hence, we try to account for the effect of an irreducible background contamination, which can only be treated by means of statistical analysis.

To begin with, in Fig. 3 we studied the effect of background/signal contribution to data. Figure 3 represents the evolution of the mean significance E(Z) as a function of $\lambda = N_s/(N_s + N_b)$, which corresponds to the fraction of WIMP events contained in the data, for three different total numbers of events $N_{\rm tot} = 25,\ 50,\ 100$. Hence, $\lambda \to 0$ means that the data are background dominated. Then, from Fig. 3, one can observe that for any total number of

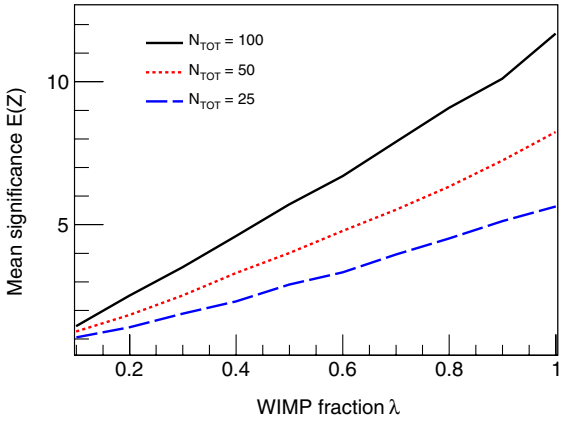

FIG. 3 (color online). Evolution of the mean significance E(Z) as a function of the expected WIMP fraction $\lambda = N_s/(N_s + N_b)$ for three different values of the expected total number of events $N_{\rm tot} = 100$ (black solid line), 50 (red dotted line), and 25 (blue long-dashed line). This study has been done by considering a WIMP mass of 50 GeV/c^2.

events, the mean significance E(Z) increases almost linearly with the data purity (λ). Also, for a given value of λ, increasing the total number of events will enhance the significance. In other words, for a given value of $\lambda = 0.5$, for example, the significance of a dark matter detection can be improved from 3σ to 6σ by having an exposure 4 times larger.

Figure 4 presents the lower bound of the 3σ discovery region at 90% C.L. ($Z_{90} = 3$ limit) in the $(m_\chi, \log_{10}(\sigma_p))$ plane. Two cases are presented: background free and high background contamination (10 $\rm kg^{-1}.year^{-1}$). For convenience, the curves of isonumber of WIMP events are presented (dashed lines) in the case of 5, 30, and 150

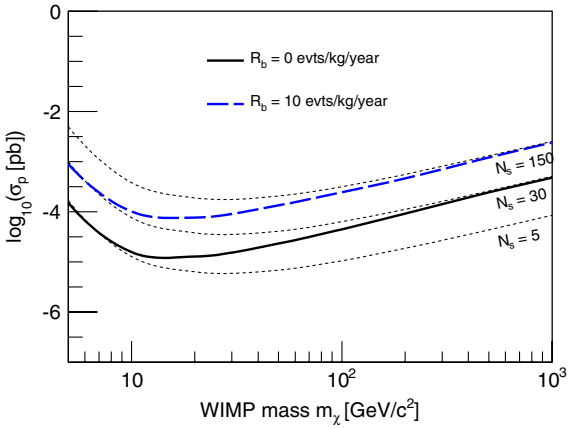

FIG. 4 (color online). Lower bound of the 3σ discovery region at 90% C.L. in the $(m_\chi, \log_{10}(\sigma_p))$ plane. Black line presents the background-free case, while the blue dashed line presents the same region with 10 background events per year per kg. For convenience, the curves of isonumber of WIMP events are presented (dashed lines) in the case of 5, 30, and 150 WIMP events.

WIMP events. One can first notice that a 30 kg.year CF_4 directional detector may allow to achieve, in the background-free case, a 3σ discovery of dark matter down to $\sim 10^{-5}$ pb at low WIMP mass (~ 10 GeV/c^2) and down to $\sim 10^{-4}$ pb for high WIMP mass (~ 1 TeV/c^2). Adding a large fraction of background in the data (10 kg^{-1}.year^{-1}) results in a loss of about 1 order of magnitude in the lower bound of the 3σ discovery region. This highlights the fact that directional detection can accommodate to a sizeable background contamination, noticing that such a background event rate in the final data set is very large. Interestingly, one may compare the 3σ lower bound to the curves of isonumber of WIMP events. At low WIMP mass (~ 10 GeV/c^2), about 5 WIMP events are enough to claim a 3σ discovery, in the background-free case, while about 30 WIMP events are needed for highly background-contaminated data. At high WIMP mass (~ 1 TeV/c^2), these numbers reach 30 and 150, respectively.

To conclude on this first study, aiming at evaluating the effect of N_s and N_b on the mean significance, one can easily appreciate the fact that using directional detection, strong evidence in favor of a dark matter detection could be reached even with low statistics and rather large background contamination. This low sensitivity to background contamination and the possibility to evaluate the dark matter and background components in the final data set give a major interest for directional detection, especially at the present stage when nondirectional experiments start to observe candidate events whose origin is difficult to assess [9–12]. On the other hand, we emphasize that, for directional detection, an unambiguous proof of discovery of Galactic dark matter would be given by a main recoil direction pointing toward the constellation Cygnus within few degrees, combined with a high significance. However, we caution that the presence of a stream or another dark matter substructure in the vicinity of the Solar System could deviate the recovering angle from the direction of the constellation Cygnus of a few degrees, depending on the relative densities, as outlined in [82].

B. Effect of the energy threshold

As for direction-insensitive direct detection, the energy threshold plays a key role for directional detection. It is worth emphasizing that it is the lowest energy at which both the initial direction and the energy of the recoiling nucleus can be retrieved, which makes it even more challenging for directional detection. In particular, this ''directional threshold'' is higher than the standard energy threshold defined as the minimal kinetic energy required for an event to be detected. Indeed, a low-energy recoil in a low-pressure TPC would present a short track length and a large angular dispersion, implying a loss of the direction information. The directional energy threshold is thus closely related to the gas pressure, the target choice, the readout performance, as well as the data analysis strategy. There are two main and competing effects when increasing the energy threshold: a reduction of the number of expected WIMP events and a selection of the most anisotropic WIMP-induced recoils.

In Fig. 5, we present the evolution of $E(Z)$ as a function of $E_{\rm th}$ for four different WIMP masses: $m_\chi = 5$ (black solid line), 10 (red dotted line), 20 (blue long-dashed line), and 50 GeV/c^2 (green short-dashed line). For the sake of comparison between the different WIMP masses, we have chosen cross section values in order to have 100 WIMP events in each case at $E_{\rm th} = 0$ keV and a constant background contamination of 10 evts/kg/year. As discussed in [6], the fact that the angular recoil distribution of WIMP events is more anisotropic at low WIMP mass comes from the fact that the energy threshold selects events at higher energies, which are the most anisotropic ones. The fact that, at $E_{\rm th} = 0$ keV, the significance is higher for lighter WIMPs is only due to the energy spectrum, which is more peaked at low energy and then more different to the background one, assumed to be flat. Then, increasing the energy threshold will decrease the number of WIMP events more rapidly in the case of light WIMPs than for heavier WIMPs and also enhance the anisotropy related to the rejection power. However, as it can be seen from Fig. 5, the significance is always decreasing with the energy threshold leading to the conclusion that the loss of WIMP events has a stronger effect on the significance than the enhancement of the anisotropy. Then, contrarily to what was predicted by [33], when looking at the whole directional event distribution $d^2R/dE_r d\Omega_r$, there is no enhancement of the significance at low-energy threshold. Of course, we caution that our result presented here suffers from energy background modeling dependence, and that

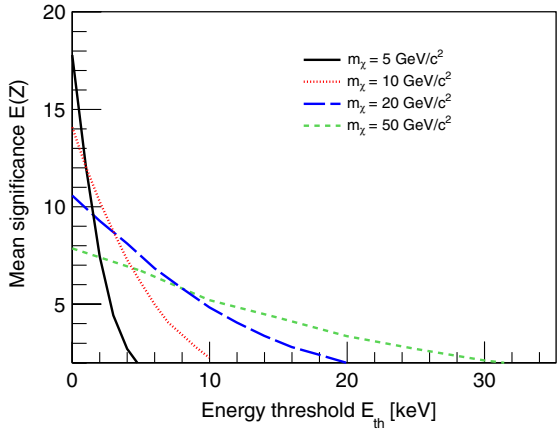

FIG. 5 (color online). Mean significance E(Z) as a function of the energy threshold, for four different WIMP masses: $m_\chi = 5$ (black solid line), 10 (red dotted line), 20 (blue long-dashed line), and 50 GeV/c^2 (green short-dashed line). We have considered a constant background rate of $R_b = 10$ evts/kg/year and different values of σ_p to get $\mu_s = 100$ events for each WIMP mass at $E_{\rm th} = 0$ keV.

for other assumptions, one could find a result similar to the one found in [33], which as been obtained by considering only the angular distribution of the events.

Figure 6 presents the lower bound of the 3σ discovery region at 90% C.L. in the $(m_\chi, \log_{10}(\sigma_p))$ for two different cases: $E_{\rm th} = 0$ keV (black solid line) and $E_{\rm th} = 50$ keV (blue long-dashed line). For convenience, the curves of isonumber of WIMP events, relevant to each case, are presented (dashed lines). One can first notice that a 30 kg.year CF_4 directional detection would allow to achieve, in the unrealistic $E_{\rm th} = 0$ keV case, a 3σ discovery of dark matter down to $\sim 10^{-5}$ pb at low WIMP mass (~ 10 GeV/c^2) and down to $\sim 10^{-4}$ pb for high WIMP mass (~ 1 TeV/c^2). At high WIMP mass, about 4 times more WIMP events are required to achieve a 3σ discovery. Considering a detector with a 50 keV energy threshold results in a loss of a factor of 5 in sensitivity at high WIMP mass and to no sensitivity at all below ~ 20 GeV/c^2.

However, as one can see from Fig. 6, the fact that, at high WIMP mass, only 15 WIMP events are required to get a 3σ discovery at 90% C.L. for $E_{\rm th} = 50$ keV while 20 are required for $E_{\rm th} = 0$ keV comes from the enhancement of the anisotropy due to the high-energy threshold.

As a conclusion of this study aiming at quantifying the impact of the energy threshold on the expected sensitivity of a given directional detection, it can simply be stated that the lower remains as expected the better. We also found that a low-energy threshold is compulsory to be sensitive to low WIMP mass. As an illustration of this statement, we found that a threshold of about 50 keV will prevent a given directional experiment, using fluorine target material, to be sensitive to very low WIMP mass $\sim$5–10 GeV/c^2. We conclude that the energy threshold remains a major experimental issue for directional detection, noticing that both the 3D track and the energy must be measured down to this energy.

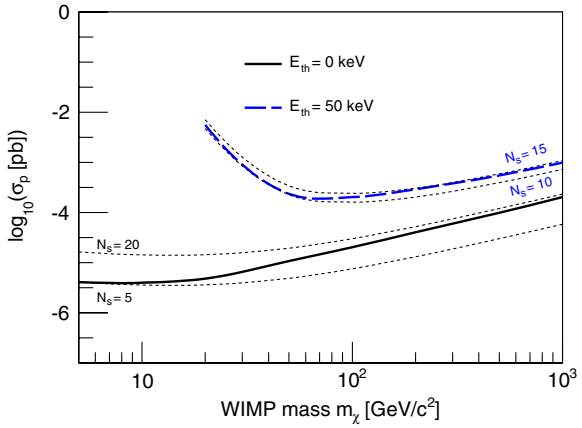

FIG. 6 (color online). Lower bound of the 3σ discovery region at 90% C.L. in the $(m_\chi, \log_{10}(\sigma_p))$ plane for two different cases: $E_{\rm th} = 0$ keV (black solid line) and $E_{\rm th} = 50$ keV (blue long-dashed line) without background events. For convenience, the curves of isonumber of WIMP events are presented in the $E_{\rm th} = 0$ keV case (black dashed lines) and in the $E_{\rm th} = 50$ keV case (blue dashed lines).

C. Effect of the sense recognition efficiency

Not only should the track be 3D reconstructed, but its sense should also be retrieved from the data analysis. As outlined in [83], an asymmetry between upgoing and downgoing tracks is expected, due to two different effects. First, the angular dispersion of recoiling tracks should result in a spatial asymmetry as the beginning of the track should be more rectilinear than its end. Second, a charge collection asymmetry is expected as the dE/dx in ionization is decreasing with energy at low-recoil energy. Hence, more primary electrons should be generated at the beginning of the track.

Even though several experimental progresses have been done [30–32], sense recognition remains a key and challenging experimental issue for directional detection of dark matter. In particular, it should still be demonstrated that sense recognition may be achieved at low-recoil energy, where most WIMP events reside.

In the following, we investigate the effect of no or partial sense recognition on the expected significance of a given directional detector. To do so, we define a sense recognition efficiency as $\epsilon_{HT} = \epsilon_G - \epsilon_W$, where ϵ_G and ϵ_W corresponds to the fraction of good and wrong reconstructed events, respectively. Then, if $\epsilon_{HT} = 0\%$, we are in the ''flipping coin'' scenario, i.e. the detector does not have any sense recognition capability. Then, the modified directional event rate that takes into account this partial sense recognition $S(\hat{R}_n)$ is defined as

$$S(\hat{R}_n) = \frac{1 + \epsilon_{HT}}{2} S(+\hat{R}_n) + \frac{1 - \epsilon_{HT}}{2} S(-\hat{R}_n), \qquad (10)$$

where $\hat{R}_n$ refers to the direction of the recoiling nucleus.

Without sense recognition, the expected WIMP-induced distribution becomes less anisotropic and thus gets closer to the expected background event distribution. This induces an obvious loss of discrimination power. Figure 7 presents the evolution of the mean significance E(Z) as a function of ϵ_{HT} for different cases ($N_s = 100$, $N_b = 0$) and ($N_s = 100$, $N_b = 100$) considering a flat energy spectrum for the background. One can notice that, for both cases, the mean significance is monotonically increasing with ϵ_{HT}. It is also shown that this significance improvement is even stronger for values of ϵ_{HT} close to 100%. It means that having ϵ_{HT} equal to 0% or to 20% does not really modify the expected significance while having ϵ_{HT} equal to 80% or to 100% changes the mean significance by almost 20%. Also, it is shown in Fig. 7 that even in the presence of a sizeable background contamination ($\lambda = 0.5$) the expected mean significance remains strong, i.e. above 5σ. Indeed, the presence of background reduces the mean significance by about 30% all over the range of ϵ_{HT}.

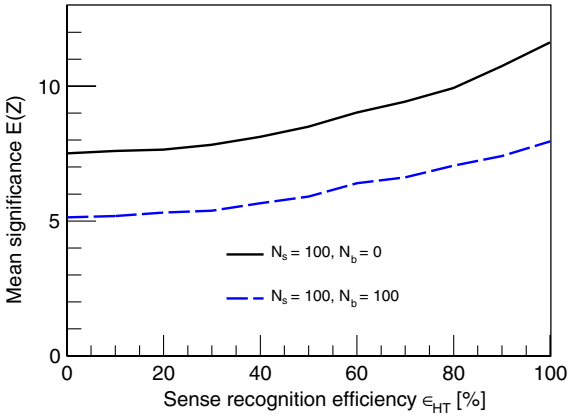

FIG. 7 (color online). Mean significance as a function of ϵ_{HT} for two different cases ($N_s = 100$, $N_b = 0$) (black solid line) and ($N_s = 100$, $N_b = 100$) (blue long-dashed line). A WIMP mass of 50 GeV/c^2 has been considered for this study.

Figure 8 presents the lower bound of the 3σ discovery region at 90% C.L. in the (m_χ, $\log_{10}(\sigma_p)$) plane for two different cases: $\epsilon_{HT} = 100\%$ (black solid line) and $\epsilon_{HT} = 0\%$ (blue long-dashed line). For convenience, the curves of isonumber of WIMP events are presented (dashed lines) in the case of 5, 30, and 120 WIMP events. One can first notice that a 30 kg.year CF_4 directional detection would allow to achieve, with full sense recognition capability, a 3σ discovery of dark matter down to $\sim 10^{-5}$ pb at low WIMP mass ($\sim$ 10 GeV/c^2) and down to $\sim 10^{-4}$–10^{-3} pb for high WIMP mass ($\sim$ 0.1–1 TeV/c^2). At high WIMP mass, about 6 times more WIMP events are required to achieve a 3σ discovery. Considering a detector with no sense-recognition capability results in a loss of a factor of 4 at high WIMP mass and almost no effect at low WIMP mass. Note that this statement depends on the background

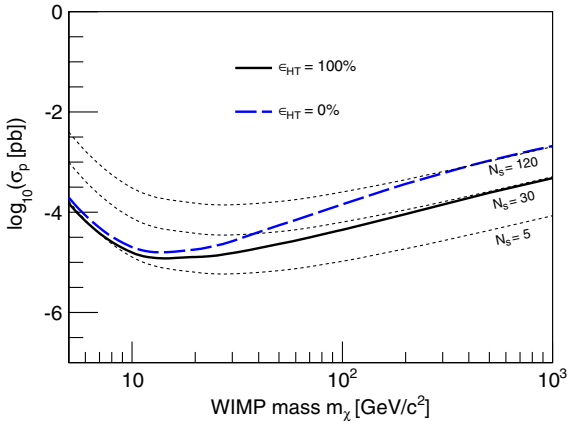

FIG. 8 (color online). Lower bound of the 3σ discovery region at 90% C.L. in the (m_χ, $\log_{10}(\sigma_p)$) plane for two different cases: $\epsilon_{HT} = 100\%$ (black solid line) and $\epsilon_{HT} = 0\%$ (blue long-dashed line) without background events. For convenience, the curves of isonumber of WIMP events are presented (dashed lines) in the case of $N_s = 5$, 30, and 120.

energy distribution (see Sec. IV F). This study leads us to the conclusion that sense recognition is not a major experimental issue. Indeed, a directional detector without sense recognition capability would still be able to achieve a 3σ discovery in the 10^{-5}–10^{-3} pb region. We emphasize that the same conclusion holds true when trying to set exclusion limits, as shown in [8]. This result is of major interest, as getting sense recognition from experimental data remains a very difficult task, probably the most difficult experimental challenge to be faced by current projects, and especially when trying to get a high sense recognition efficiency down to the energy threshold.

D. Effect of angular resolution

As far as directional detection is concerned, the estimation of the initial recoil direction is compulsory. This gives an intrinsic limitation of this detection strategy as recoil tracks in low-pressure gaseous detectors would encounter a rather large angular dispersion ("straggling" effect) by colliding with other nuclei of the gas. Moreover, the gas properties imply a transverse and longitudinal diffusion of the primary electrons that will contribute to the angular resolution. Hence, data of upcoming directional detectors should suffer from rather large angular resolution. Having a finite angular resolution means that a recoil initially coming from the direction $\hat{r}(\Omega_r)$ is reconstructed as a recoil coming from the direction $\hat{r}'(\Omega_r')$ with a Gaussian dispersion of width σ_γ according to the following distribution:

$$K(\Omega_r, \Omega_r') = e^{-\gamma^2/2\sigma_\gamma^2}/((2\pi)^{2/3}\sigma_\gamma \mathrm{erf}(\sqrt{2}\sigma_\gamma)), \quad (11)$$

where the angle γ between the $\hat{r}(\Omega_r)$ and $\hat{r}'(\Omega_r')$ is defined by

$$\cos\gamma = \cos b_r \cos b_r' \cos(l_r - l_r') + \sin b_r \sin b_r', \quad (12)$$

where the angles l and b refer to the Galactic coordinates.

The directional recoil rate is then given by the convolution product of the initial recoil rate and the angular distribution as

$$\frac{d^2R}{d\Omega_r dE_r}(\Omega_r, E_r) = \int_{\Omega_r'} \frac{d^2R}{d\Omega_r dE_r}(\Omega_r', E_r) K(\Omega_r, \Omega_r') d\Omega_r'. \quad (13)$$

The evolution of the expected mean significance E(Z) as a function of the angular resolution σ_γ is shown on Fig. 9. Two different cases are considered ($N_s = 100$, $N_b = 0$) (black solid line) and ($N_s = 100$, $N_b = 100$) (blue long-dashed line) with a flat background. As one can see, for each configuration, degrading the angular resolution (i.e. increasing σ_γ) results in a diminution of the expected mean significance. This comes from the fact that for large angular values of the angular resolution, the angular distribution of the expected WIMP events is less anisotropic and is getting closer to the angular distribution of

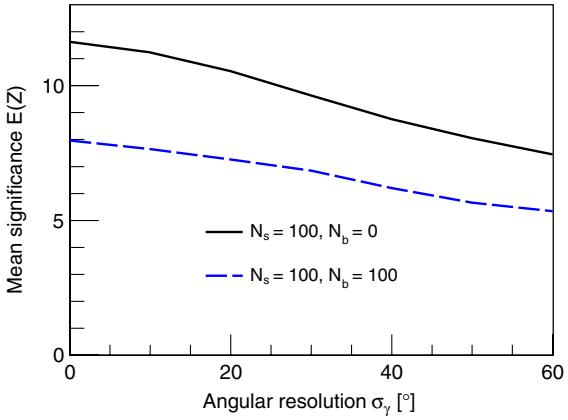

FIG. 9 (color online). Mean significance as a function of the angular resolution σ_γ for different cases ($N_s = 100$, $N_b = 0$) (black solid line) and ($N_s = 100$, $N_b = 0$) (blue long-dashed line). A WIMP mass of 50 GeV/c^2 has been considered for this study.

background events, which is isotropic. From Fig. 9, we can see that an angular resolution of $\sigma_\gamma = 60°$ decreases the mean significance of about 30% in comparison to the case where $\sigma_\gamma = 0°$.

The effect of angular resolution on the expected discovery potential of a directional detection experiment is shown on Fig. 10. Indeed, we have represented in the ($\log_{10}(\sigma_p)$, m_χ) plane the 90% C.L. limit to reach a dark matter detection with a significance greater or equal to 3σ considering a perfect angular resolution (black solid line) and $\sigma_\gamma = 60°$ (blue long-dashed line). For convenience, the black dashed line corresponds to isovalue of expected WIMP events for $N_s = 5$, 30, and 100. As one can see, the effect of an angular resolution of 60° is very small at low WIMP mass due to the fact that at low WIMP mass the

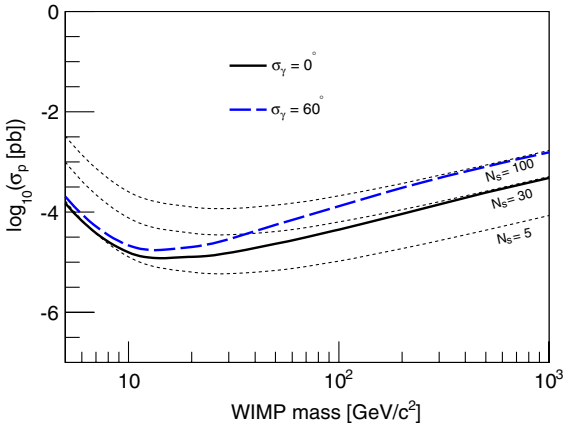

FIG. 10 (color online). Lower bound of the 3σ discovery region at 90% C.L. in the (m_χ, $\log_{10}(\sigma_p)$) plane for two different cases: $\sigma_\gamma = 0°$ (black solid line) and $\sigma_\gamma = 60°$ (blue long-dashed line) without background events. For convenience, the curves of isonumber of WIMP events are presented (dashed lines) in the case of 5, 30, and 100 WIMP events.

expected angular distribution is much more anisotropic than for heavy WIMPs. Then, at high WIMP mass, the effect of angular resolution is non-negligible as we found a reduction in the sensitivity of about a factor of 3.3. This result suggests that directional detection should still be very competitive even with a rather poor angular resolution. It may be noticed from Fig. 8 and Fig. 10 that the effect of an angular resolution of 60° with $\epsilon_{HT} = 100\%$ is almost equivalent to not having the sense recognition capability with a perfect angular resolution.

Then, as for the sense recognition study, we can conclude that angular resolution is not a major experimental issue. Indeed, a low-angular-resolution detector would still be able to achieve a 3σ discovery in the 10^{-5}–10^{-3} pb region.

E. Effect of the energy resolution

Low pressure gaseous TPC detectors allow the ionization energy to be measured. It should then be converted to a recoil energy thanks to the knowledge of the ionization quenching factor. The measurement of this quantity is a major issue for directional detection with gaseous TPC [84,85].

So far, we have considered a directional detector with a perfect energy resolution. In this section, we present the effect of a nonperfect energy resolution on the expected sensitivity of a directional detector. As outlined above, most directional detection experiments are TPCs, and they will hence be affected by energy resolutions much higher than the ones from cryogenic detectors, for instance.

The energy resolution on the recoil energy σ_{E_r} is taken into account in the expected directional recoil rate distribution using the following procedure:

$$\frac{d^2R}{d\Omega_r dE_r}(\Omega_r, E_r) = \int_{E'_r} \frac{d^2R}{d\Omega_r dE_r}(\Omega_r, E'_r) \times \frac{1}{\sqrt{2\pi}\sigma(E'_r)} \times \exp\left\{-\frac{1}{2}\left(\frac{E_r - E'_r}{\sigma(E'_r)}\right)^2\right\} dE'_r. \quad (14)$$

Having a nonperfect energy resolution will lead to two different effects that are in competition. The first one is that it will enhance the expected number of WIMP events. Indeed, as most of the WIMP events lie at low energy, if the energy resolution (σ_{E_r}) is large, low-energy events could pass the energy threshold and be detected. The second effect is that it will smooth the energy distribution leading to a WIMP event energy distribution closer to the expected background one (flat) and then reduce the discrimination power.

The effect of energy resolution is shown in Fig. 11, which presents the evolution of the mean expected significance E(Z) as a function of σ_{E_r}. The latter presents the results obtained in the cases of a 20 GeV/c^2 (black lines) and 100 GeV/c^2 (blue lines) WIMP mass considering ($N_s = 100$, $N_b = 0$) (solid lines) and ($N_s = 100$,

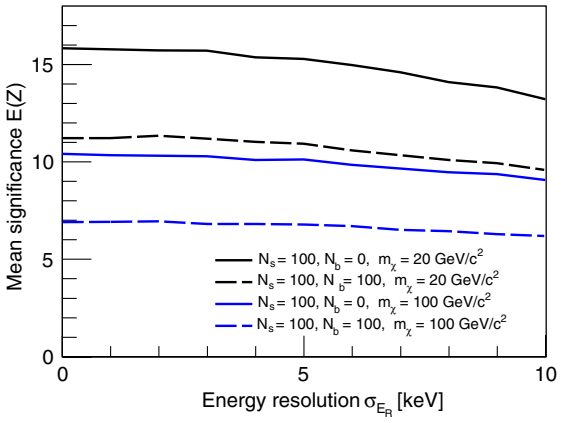

FIG. 11 (color online). Mean significance as a function of σ_{E_r} for different cases ($N_s = 100$, $N_b = 0$) (solid lines) and ($N_s = 100$, $N_b = 100$) (long-dashed lines) according to two different WIMP masses: $m_\chi = 20$ GeV/c^2 (black lines) and $m_\chi = 100$ GeV/c^2 (blue lines).

$N_b = 100$) (long-dashed lines). We have considered value for σ_{E_r} ranging from 0 keV, i.e. perfect energy resolution, to 10 keV. As the recoil energy range of the detector is taken, for this example, between 5 and 50 keV, $\sigma_{E_r} =$ 10 keV corresponds to an extreme and unrealistic energy resolution of 200% at 5 keV and 20% at 50 keV. However, as one can see from Fig. 11, even with an extremely large energy resolution, the mean expected significance is only slightly degraded compared to the case of a perfect energy resolution, i.e. 15% in the case $m_\chi = 20$ GeV/c^2 and ($N_s = 100$, $N_b = 0$) (black solid line). From Fig. 11, we can also appreciate the fact that the effect of energy resolution on the significance of a dark matter detection is negligible even with a 50% background contribution and for a 100 GeV/c^2 WIMP mass.

As a conclusion of this study, we have shown that energy resolution is a meaningless experimental issue for the dark matter sensitivity of a given directional detector.

F. Effect of the background energy model

The last experimental issue to be discussed is the effect of energy background modeling on the estimation of the sensitivity of a directional detector. In the previous sections, we have considered a directional event rate for background events flat in energy. Then, in this section, we consider an exponential background energy spectrum in the form of

$$\left.\frac{dR}{dE_r}\right|_{\text{back}} = -\frac{1}{E_{\text{back}}} \times \frac{\exp(-E_r/E_{\text{back}})}{\exp(-E_{\text{th}}/E_{\text{back}})}, \qquad (15)$$

where E_{back} refers to the slope of the background energy distribution and if $E_{\text{back}} \to +\infty$ we recover a flat energy spectrum. Obviously, the worst scenario is when the expected WIMP event energy distribution and the background one are the same. Indeed, in such case, there is no more discrimination between WIMP events and background events based on the energy information. For concreteness, we exemplify this statement by considering the case $E_{\text{back}} = 17.4$ keV, corresponding to the slope expected for WIMP-induced recoil energy distribution when considering a WIMP mass of 50 GeV/c^2 and fluorine target. In Figs. 12 and 13, one can see the evolution of E(Z) as a function of E_{back} for different values of ϵ_{HT} and σ_γ. The common feature is that E(Z) is maximal at very low value of E_{back} corresponding to a very steep background energy spectrum, then decreases to a minimal value located around $E_{\text{back}} = 17.4$ keV and then increases asymptotically to the case where $E_{\text{back}} \to +\infty$ corresponding to a flat background energy spectrum. An interesting

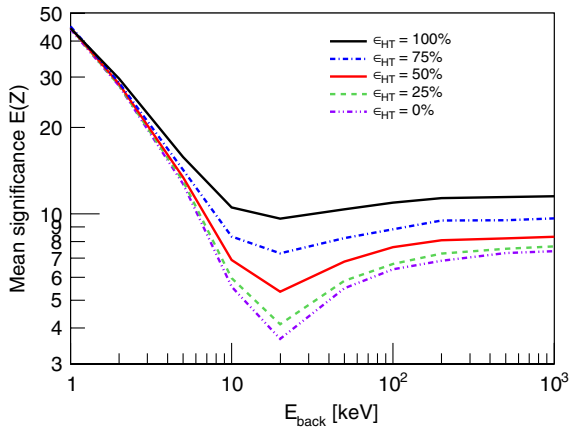

FIG. 12 (color online). Mean significance as a function of the background slope E_{back} for 5 different values of sense recognition efficiencies (from top to bottom): $\epsilon_{HT} = 100\%$, 75%, 50%, 25%, and 0%. A WIMP mass of 50 GeV/c^2 with 100 expected WIMP events and no background contamination has been considered in this study.

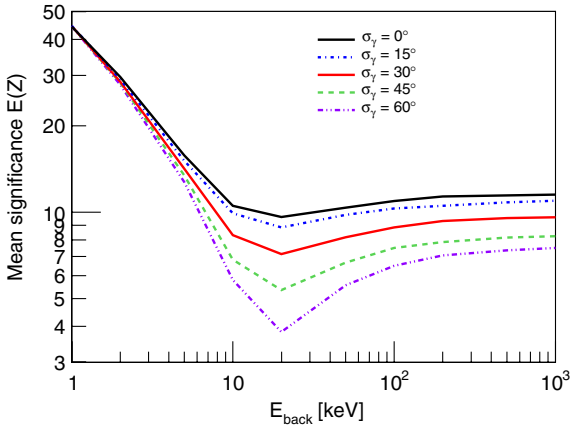

FIG. 13 (color online). Mean significance as a function of the background slope E_{back} for 5 different values of angular resolution (from top to bottom): $\sigma_\gamma = 0°$, 15°, 30°, 45°, and 60°. A WIMP mass of 50 GeV/c^2 with 100 expected WIMP events and no background contamination has been considered in this study.

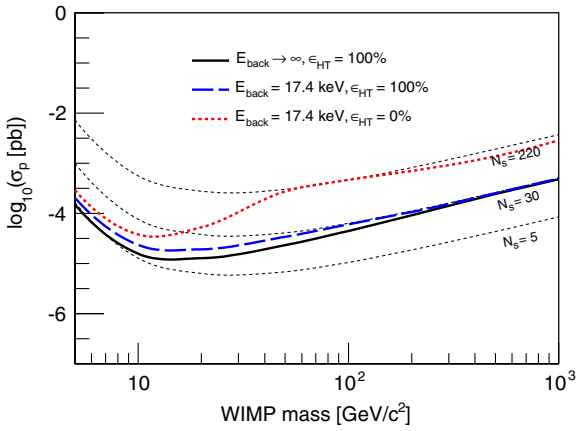

FIG. 14 (color online). Lower bound of the 3σ discovery region at 90% C.L. in the $(m_\chi, \log_{10}(\sigma_p))$ plane for three different cases: ($E_{\text{back}} \rightarrow +\infty$ keV, $\epsilon_{HT} = 100\%$) (black solid line), ($E_{\text{back}} = 17.4$ keV, $\epsilon_{HT} = 100\%$) (blue long-dashed line), and ($E_{\text{back}} = 17.4$ keV, $\epsilon_{HT} = 0\%$) (red dotted line) without background events. For convenience, the curves of isonumber of WIMP events are presented (dashed lines) in the case of 5, 30, and 220 WIMP events.

point that should be highlighted is the fact that the effect of E_{back} on the expected sensitivity depends strongly on the angular performance of the detector. Indeed, the minimal value of E(Z) at $E_{\text{back}} = 17.4$ keV is strongly degraded when decreasing the sense recognition efficiency or increasing the angular resolution. This is simply explained by the fact that, for this particular value of the background slope exactly equal to the WIMP-induced event slope, the discrimination between WIMP and background events relies only on the angular information.

Finally, the effect of energy background modeling on the expected discovery potential of a given directional detector is shown in Fig. 14. We have presented, on the $(m_\chi, \log_{10}(\sigma_p))$ plane, the lower bound of the 3σ discovery region at 90% C.L. in three different cases: flat background energy spectrum ($E_{\text{back}} \rightarrow +\infty$) with $\epsilon_{HT} = 100\%$ (black solid line), $E_{\text{back}} = 17$ keV with $\epsilon_{HT} = 100\%$ (blue long-dashed line), and $E_{\text{back}} = 17$ keV with $\epsilon_{HT} = 0\%$ (red dotted line). Taken at face value, these results suggest that the effect of the background energy distribution is negligible in the case of a high-performance tracking device but can be significant if the angular resolution and/or sense recognition efficiency are poor. Indeed, as one can see from the red dotted line in Fig. 14, the sensitivity is degraded by almost 1 order of magnitude when the WIMP mass corresponds to the considered value of E_{back} and if the detector does not have sense recognition.

V. PROSPECT

In this last section, we are interested in evaluating the discovery potential of two very different directional experiments referred to as detector A and B, see Table II. Both of them are considered as 10 kg of CF_4 time projection chambers operated during three years with three-dimensional track reconstruction. High-performance characteristics are considered for detector A, while detector B stands for the pessimistic case. Indeed, the detector A will be considered with an energy threshold of 5 keV, with an angular resolution of 20°, a 100% sense recognition efficiency, and no background contamination; while detector B is characterized by an energy threshold of 20 keV, an angular resolution of 50°, no sense recognition capability, and a high background contamination of 10 events/kg/year uniformly distributed in energy. This way, detector B can be considered as a pessimistic scenario and detector A as an optimistic one that could also be interpreted as the ultimate directional detector.

TABLE II. Characteristics of the two detectors A and B considered.

	E_{th} [keV]	R_b [events/kg/year]	σ_γ [°]	ϵ_{HT} [%]
Detector A	5	0	20	100
Detector B	20	10	50	0

In Fig. 15, we present the lower bound of the 3σ discovery region at 90% C.L. in the $(m_\chi, \log_{10}(\sigma_p))$ plane corresponding to the detectors A (red solid line) and B (blue solid line). For comparison with other direct

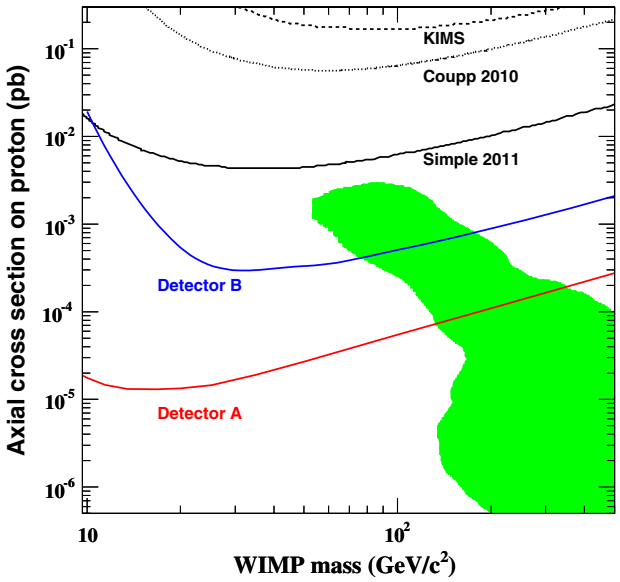

FIG. 15 (color online). Lower bound of the 3σ discovery region at 90% C.L. in the $(m_\chi, \log_{10}(\sigma_p))$ plane for the two detectors A (red solid line) and B (blue solid line), considering a 30 kg.year exposure. The theoretical region, obtained within the framework of the constrained minimal supersymmetric model, is taken from [87] and shown as the green contour. Constraints from collider data and relic abundance are accounted for. Exclusion limits from direct searches are also shown: SIMPLE [13] (black solid line), COUPP [14] (dotted line), and KIMS [16] (dashed line).

searches, we have reported current limits from SIMPLE [13] (black solid line), COUPP [14] (black dashed line), and KIMS [16] (black dotted line). All limits are given in the pure-proton approximation [86]. To evaluate the discovery potential of dark matter corresponding to the detectors A and B, we have reported the theoretical region obtained within the framework of the constrained minimal supersymmetric model, taken from [87], as the green contour.

The first result that can be inferred from Fig. 15 is that the sensitivity of detector A is about 1 order of magnitude below the one from detector B for WIMP masses above 50 GeV/c^2 and about 3 orders of magnitude for $m_\chi =$ 10 GeV/c^2. This highlights the need for detector optimization and to justify a substantial experimental effort on directional detection to reach a high-performance detector. It also means that, contrarily to detector A, detector B will not be sensitive to light WIMP below $\sim$20 GeV/c^2. The second result is that both detector A and B are competitive as they are 1 and 2 orders of magnitude below current exclusion limits. Moreover, both of them should be able to reach a large part of the predicted supersymmetric model, which is motivated both by particle physics and cosmological constraints. Hence, even a low-performance directional detector, with a 30 kg.year exposure, could allow to identify WIMP events as such by recovering, with a high significance, the main incoming direction of the events.

VI. CONCLUSION

In this paper, we have shown that the use of a profile likelihood ratio test statistic is very well suited when trying to estimate the sensitivity of a given directional experiment. Indeed, it allows us to propagate, using a frequentist approach, some astrophysical uncertainties that are very important in the field of direct searches of dark matter. This way, we have studied one by one the impact on the sensitivity of most of the experimental issues related to directional detection in the goal of directional detection optimization. We have then been able to elaborate a weighted wish list where we found that the energy threshold and the background contamination are the most dominant effect. About the effect of angular resolution and sense recognition efficiency, we found that they could affect strongly (about a factor of 4–5) the sensitivity of a directional experiment especially at high WIMP mass $m_\chi > 100$ GeV/c^2. On the other hand, we found that the energy resolution of the detector affects the sensitivity only in a negligible way, even in extreme and unrealistic cases. However, detector commissioning is compulsory to derive relevant exclusion limits or discovery regions.

Finally, we found that directional detection with a 10 kg CF_4 time projection chamber should be able to reach an important part of supersymmetric models and be competitive with current experimental limits, even in the case of a directional experiment with very low performance. Hence, we believe that directional detection of dark matter is a very promising direct search for dark matter that should be able to clearly authenticate a genuine positive detection with a high significance.

ACKNOWLEDGMENTS

J. B. would like to thank Benoit Clement and Glen Cowan for fruitful discussions and valuable advice concerning the profile likelihood ratio test statistic.

[1] E. Komatsu *et al.*, Astrophys. J. Suppl. Ser. **192**, 18 (2011).
[2] M. Persic, P. Salucci, and F. Stel, Mon. Not. R. Astron. Soc. **281**, 27 (1996).
[3] A. Klypin, H. Zhao, and R. S. Somerville, Astrophys. J. **573**, 597 (2002).
[4] D. N. Spergel, Phys. Rev. D **37**, 1353 (1988).
[5] A. M. Green and B. Morgan, Phys. Rev. D **81**, 061301 (2010).
[6] J. Billard, F. Mayet, J. F. Macias-Perez, and D. Santos, Phys. Lett. B **691**, 156 (2010).
[7] J. Billard, F. Mayet, and D. Santos, Phys. Rev. D **83**, 075002 (2011).
[8] J. Billard, F. Mayet, and D. Santos, Phys. Rev. D **82**, 055011 (2010).
[9] Z. Ahmed *et al.*, Phys. Rev. D **84**, 011102 (2011).
[10] E. Aprile *et al.*, Phys. Rev. Lett. **107**, 131302 (2011).
[11] C. E. Aalseth *et al.*, Phys. Rev. Lett. **106**, 131301 (2011).
[12] G. Angloher *et al.*, arXiv:1109.0702.
[13] M. Felizardo *et al.*, arXiv:1106.3014.
[14] E. Behnke *et al.*, Phys. Rev. Lett. **106**, 021303 (2011).
[15] A. Benoit *et al.*, Phys. Lett. B **616**, 25 (2005).
[16] H. S. Lee *et al.*, Phys. Rev. Lett. **99**, 091301 (2007).
[17] G. J. Alner *et al.*, Phys. Lett. B **616**, 17 (2005).
[18] S. Archambault *et al.*, Phys. Lett. B **682**, 185 (2009).
[19] J. Angle *et al.*, Phys. Rev. Lett. **101**, 091301 (2008).
[20] V. N. Lebedenko *et al.*, Phys. Rev. Lett. **103**, 151302 (2009).
[21] G. Cowan, K. Cranmer, E. Gross, and O. Vitells, Eur. Phys. J. C **71**, 1554 (2011).
[22] E. Aprile *et al.*, Phys. Rev. D **84**, 052003 (2011).
[23] S. Ahlen *et al.*, Int. J. Mod. Phys. A **25**, 1 (2010).
[24] K. Miuchi *et al.*, Phys. Lett. B **686**, 11 (2010).
[25] E. Daw *et al.*, arXiv:1010.3027.
[26] S. E. Vahsen *et al.*, arXiv:1110.3401.
[27] S. Ahlen *et al.*, Phys. Lett. B **695**, 124 (2011).
[28] T. Naka *et al.*, arXiv:1109.4485.
[29] D. Santos *et al.*, J. Phys. Conf. Ser. **309**, 012014 (2011).

[30] D. Dujmic *et al.*, Nucl. Instrum. Methods Phys. Res., Sect. A **584**, 327 (2008).
[31] P. Majewski, D. Muna, D. P. Snowden-Ifft, and N. J. C. Spooner, Astropart. Phys. **34**, 284 (2010).
[32] S. Burgos *et al.*, arXiv:0809.1831.
[33] A. M. Green and B. Morgan, Astropart. Phys. **27**, 142 (2007).
[34] M. S. Alenazi and P. Gondolo, Phys. Rev. D **77**, 043532 (2008).
[35] P. D. Serpico and G. Bertone, Phys. Rev. D **82**, 063505 (2010).
[36] A. M. Green, J. Cosmol. Astropart. Phys. 10 (2010) 034.
[37] N. W. Evans, C. M. Carollo, and P. T. de Zeeuw, Mon. Not. R. Astron. Soc. **318**, 1131 (2000).
[38] P. Gondolo, Phys. Rev. D **66**, 103513 (2002).
[39] J. D. Lewin and P. F. Smith, Astropart. Phys. **6**, 87 (1996).
[40] F. S. Ling, E. Nezri, E. Athanassoula, and R. Teyssier, J. Cosmol. Astropart. Phys. 02 (2010) 012.
[41] C. McCabe, Phys. Rev. D **82**, 023530 (2010).
[42] M. Kuhlen, N. Weiner, J. Diemand, P. Madau, B. Moore, D. Potter, J. Stadel, and M. Zemp, J. Cosmol. Astropart. Phys. 02 (2010) 030.
[43] P. J. Fox, J. Liu, and N. Weiner, Phys. Rev. D **83**, 103514 (2011).
[44] P. J. Fox, G. D. Kribs, and T. M. P. Tait, Phys. Rev. D **83**, 034007 (2011).
[45] L. E. Strigari and R. Trotta, J. Cosmol. Astropart. Phys. 11 (2009) 019.
[46] D. G. Cerdeno and A. M. Green, In *Particle dark matter: Observations, Models and Searches*, edited by G. Bertone (Cambridge University Press, Cambridge, England, 2010).
[47] A. M. Green, arXiv:1004.2383.
[48] C. Amsler *et al.* (Particle Data Group), Phys. Lett. B **667**, 1 (2008).
[49] E. I. Gates, G. Gyuk, and M. S. Turner, Astrophys. J. **449**, L123 (1995).
[50] P. Salucci, F. Nesti, G. Gentile, and C. F. Martins, Astron. Astrophys. **523**, A83 (2010).
[51] M. Weber and W. de Boer, Astron. Astrophys. **509**, A25 (2010).
[52] R. Catena and P. Ullio, J. Cosmol. Astropart. Phys. 08 (2010) 004.
[53] S. Garbari, J. I. Read, and G. Lake, arXiv:1105.6339 [Mon. Not. R. Astron. Soc. (to be published)].
[54] M. C. Smith, S. H. Whiteoak, and N. W. Evans, arXiv:1111.6920 [Astrophys. J. (to be published)].
[55] D. M. Bramich *et al.*, Mon. Not. R. Astron. Soc. **386**, 887 (2008).
[56] M. Pato, O. Agertz, G. Bertone, B. Moore, and R. Teyssier, Phys. Rev. D **82**, 023531 (2010).
[57] M. Vogelsberger *et al.*, Mon. Not. R. Astron. Soc. **395**, 797 (2009).
[58] F. J. Kerr and D. Lynden-Bell, Mon. Not. R. Astron. Soc. **221**, 1023 (1986).
[59] C. J. Copi, L. M. Krauss, D. Simmons-Duffin, and S. R. Stroiney, Phys. Rev. D **75**, 023514 (2007).
[60] M. J. Reid *et al.*, Astrophys. J. **700**, 137 (2009).
[61] P. J. McMillan and J. J. Binney, Mon. Not. R. Astron. Soc. **402**, 934 (2010).
[62] J. Bovy, D. W. Hogg, and H. Rix, Astrophys. J. **704**, 1704 (2009).
[63] S. E. Koposov, H.-W. Rix, and D. W. Hogg, Astrophys. J. **712**, 260 (2010).
[64] M. Feast and P. Whitelock, Mon. Not. R. Astron. Soc. **291**, 683 (1997).
[65] A. M. Ghez *et al.*, Astrophys. J. **689**, 1044 (2008).
[66] S. Gillessen *et al.*, Astrophys. J. **692**, 1075 (2009).
[67] A. M. Green, J. Cosmol. Astropart. Phys. 08 (2007) 022.
[68] F. S. Ling, Phys. Rev. D **82**, 023534 (2010).
[69] T. Bruch, J. Read, L. Baudis, and G. Lake, Astrophys. J. **696**, 920 (2009).
[70] J. I. Read, G. Lake, O. Agertz, and V. P. Debattista, Mon. Not. R. Astron. Soc. **389**, 1041 (2008).
[71] P. B. Tissera *et al.*, Mon. Not. R. Astron. Soc. **406**, 922 (2010).
[72] D. R. Law, S. R. Majewski, and K. V. Johnston, Astrophys. J. **703**, L67 (2009).
[73] E. Hayashi, J. F. Navarro, and V. Springel, Mon. Not. R. Astron. Soc. **377**, 50 (2007).
[74] S. H. Hansen and B. Moore, New Astron. Rev. **11**, 333 (2006).
[75] M. C. Smith *et al.*, Mon. Not. R. Astron. Soc. **399**, 1223 (2009).
[76] J. Binney and S. Tremaine, *Galactic Dynamics* (Princeton University, Princeton, NJ, 2008).
[77] B. Moore, C. Calcaneo-Roldan, J. Stadel, T. R. Quinn, G. Lake, S. Ghigna, and F. Governato, Phys. Rev. D **64**, 063508 (2001).
[78] M. Vogelsberger *et al.*, Mon. Not. R. Astron. Soc. **395**, 797 (2009).
[79] R. Teyssier, Astron. Astrophys. **385**, 337 (2002).
[80] M. C. Smith *et al.*, Mon. Not. R. Astron. Soc. **379**, 755 (2007).
[81] G. Cowan, *Statistical Data Analysis* (Clarendon, Oxford, 1998).
[82] B. Morgan, A. M. Green, and N. J. C. Spooner, Phys. Rev. D **71**, 103507 (2005).
[83] J. Billard, F. Mayet, and D. Santos, arXiv:1110.0955.
[84] O. Guillaudin *et al.*, arXiv:1110.2042.
[85] D. Santos *et al.*, arXiv:0810.1137.
[86] D. R. Tovey *et al.*, Phys. Lett. B **488**, 17 (2000).
[87] R. Trotta, F. Feroz, M. P. Hobson, L. Roszkowski, and R. Ruiz de Austri, J. High Energy Phys. 12 (2008) 024.